RESEARCH ARTICLE

Saturated Switching Functions for Sliding Mode Control With Speed Error Limitation

DENIS VASKO , JÁN KARDOŠ , EVA MIKLOVIČOVÁ , AND ĽUBOŠ CHOVANEC

Institute of Robotics and Cybernetics, Faculty of Electrical Engineering and Information Technology, Slovak University of Technology in Bratislava (STU), 841 04 Bratislava, Slovakia

Corresponding author: Denis Vasko (denis.vasko@stuba.sk)

ABSTRACT The saturated non-singular terminal switching function (SNTSF) for sliding mode control with speed error limitation and finite-time error convergence is proposed. The sliding-mode dynamics and the boundary layer dynamics of the SNTSF are analyzed. It is also shown that the non-singular terminal switching function does not have a higher boundary layer position tracking precision than the linear switching function, contrary to some previous claims in the literature. An SNTSF sliding mode controller with speed error limitation and finite-time convergence is proposed and tested both simulatively and experimentally on a laboratory DC motor system.

INDEX TERMS Boundary layer, finite-time, nonlinear control, non-singular, saturation, sliding mode, error speed limitation, terminal.

I. INTRODUCTION

The control of real-world nonlinear uncertain systems with disturbances necessitates the use of robust control approaches. Sliding mode control (SMC) [1], [2], [3] is one such approach, with good disturbance rejection capability and often simple implementation.

The design of a sliding mode controller may be broken up into two phases: the design of the switching function s and the derivation of the control law u, which drives the switching function value to zero as time progresses.

In the first part of the design, the surface $s = 0$ is chosen, such that $s = 0$ corresponds to the compensated dynamics [4] (or reference dynamics). Since $s = 0$ defines the compensated dynamics, then the choice of the surface $s = 0$ is important and many classes of switching functions have been introduced and classified into broad categories [5]. The most common ones are the linear switching function [6], the non-singular terminal switching function [3], [7], [8] and their combinations [9], [10], [11]. One of the more recently introduced switching functions is the compound switching

function in [12]. The compensated dynamics of this switching function results in convergence with speed error limitation.

The second step of SMC design is control law synthesis. The control law has to ensure that the switching function converges to 0 even in the presence of disturbances, which may necessitate the use of discontinuous control, which may introduce unwanted oscillations and chattering [13]. The simplest solution to this problem is the introduction of a so-called boundary layer [14]. When a boundary layer is used, the switching function s need not converge to 0, but only into an interval of the form $[-\Delta_s, \Delta_s]$ with $\Delta_s > 0$. In this case, the plant does not acquire the compensated dynamics, but only the quasi-compensated dynamics [4].

In the case of specific second order systems and the linear switching function the "steady-state" position errors are proportional to the width of the boundary layer Δ_s [7] and in the case of the (singular) terminal switching function the same errors are proportional to $\Delta_s^{p/q}$ [8], where $p/q > 1$, which leads to more precise position tracking for small Δ_s.

The following is a short summary of this paper.

In Section II the concept of resting intervals is introduced. This allows rigorous description of "steady-state" error bounds.

The associate editor coordinating the review of this manuscript and approving it for publication was Feiqi Deng .

The main results of this paper are in sections III, IV, V and VI.

In section III the speed error limiting switching function from [12] is rewritten using a single equation and some of its dynamic properties are analyzed and proven. The resulting switching function is given the name saturated linear switching function.

In section IV the saturated non-singular terminal switching function is defined an analyzed. This switching function shares the speed error limitation property of its saturated linear counterpart, but it also possesses finite-time convergence properties.

The non-singular terminal switching function should possess a narrower "steady-state" position error bound [7] when a boundary layer is used to suppress chattering [14]. In section V it is shown, that this is not the case.

In section VI a saturated non-singular terminal switching function based controller is synthesized for an uncertain second order system. Control performance is verified simulatively and experimentally, and compared to controllers that are based on switching functions from [6], [7] and [12].

II. RESTING INTERVALS
Since the term "steady-state position (speed) error" or "steady-state (speed) error bound" are imprecise, and since these bounds are often referred to in this paper, it seems necessary to adopt a more precise definition of these terms.

For this reason, the concept of resting intervals is defined here and used in the rest of the paper.

Definition 1: A closed interval C is a resting interval of the scalar-valued function $e(s, t)$ over $s \in S$, if and only if for all $s(t) \in S$ and any $\epsilon > 0$, there is a t_0, such that for all $t > t_0$ it is true that $\min_{c \in C} |e(s, t) - c| < \epsilon$.

The definition of the resting interval, may also be written using the limit notation as

$$\lim_{t \to \infty} \min_{c \in C} |e(s(t), t) - c| = 0 \text{ for all } s(t) \in S. \quad (1)$$

Loosely speaking, $e(s(t), t)$ converges into the set C asymptotically, for all possible $s(t) \in S$.

Any interval that contains a resting interval is also a resting interval. A resting interval that does not contain a proper subinterval that is also a resting interval is the "smallest" resting interval, defined as follows.

Definition 2: If for every proper closed subinterval I_s of a resting interval I of $e(s, t)$ over $s \in S$ and every t_0, there is an $s(t) \in S$ and a $t_1 > t_0$, such that $e(s(t_1), t_1) \neq I_s$, then I is the smallest resting interval of $e(s, t)$ over $s \in S$.

This definition states that for every closed subinterval I_s of I it is "always" possible to choose some $s(t)$ from S such that $e(t)$ will leave I_s at some future time t_1. The fact that $s(t)$ may be chosen for each I_s independently, reflects the fact that the true value of $s(t)$ is not known and therefore it is not possible to "commit" to any particular $s(t)$, even though there may be some $s(t) \in S$ for which $e \to I_s \subset I$ for $t \to \infty$.

The following lemma gives a sufficient condition to make I the smallest resting interval of $e(s, t)$ over $s \in S$ according to the previous definition.

Lemma 1: If for every closed subinterval I_s of a resting interval I of $e(s, t)$ over $s \in S$ there exists an $s(t) \in S$ and a constant $\epsilon \in I$ such that $\epsilon \notin I_s$ and

$$\lim_{t \to \infty} e(s(t), t) = \epsilon, \quad (2)$$

then I is the smallest resting interval of $e(s, t)$ over $s \in S$.

Proof: Since $\epsilon \in I = [i_1, i_2]$ and $\epsilon \notin I_s = [i_{s,1}, i_{s,2}]$ and I_s is a proper closed subinterval of I, then there is an ϵ_2 such that

1) $i_{s,2} < \epsilon_2 < \epsilon < i_2$
2) or $i_1 < \epsilon < \epsilon_2 < i_{s,1}$,

and since there is an $s(t)$ such that $\lim_{t \to \infty} e(s(t), t) = \epsilon$, then for this $s(t)$ and for all t_0 there is a $t_1 > t_0$, such that $|e(s(t_1), t_1) - \epsilon| < |\epsilon_2 - \epsilon|$ based on which $e(s(t_1), t_1) \notin I_s$ for both cases 1 and 2. ■

These definitions and lemma are used later in this paper, when the boundary layer properties of the saturated sliding functions are analyzed.

III. THE SATURATED LINEAR SWITCHING FUNCTION
It is assumed, that e represents position error, the limit $\dot{e} = de/dt$ exists and represents speed error, a, k are constants and the saturation function is defined by

$$\text{sat}(\cdot) = \max(-1, \min(1, \cdot)). \quad (3)$$

Function arguments are left out for the sake of brevity, e.g. e is written instead of $e(t)$ etc.

The following switching function definition can found in block diagram form in [12]:

$$s = \dot{e} + a\,\text{sat}(ke). \quad (4)$$

This saturated linear switching function (SLSF) already appears in [12], but is not explicitly stated as a single equation.

The contour and surface plots of (4) for $a = 1$ and $k = 1$ are shown in Fig. 1. Some figures in this paper were made with Asymptote [15].

The main purpose of using (4) as a switching function is to implement speed error limitation [12], which allows steeper switching line slopes without introducing overshoot into systems with control input limitations, which may lead to more precise position tracking. An additional effect is the reduction of dependence of $|s|$ on e, i.e. $|s|$ is bounded for bounded $\dot{e}$ regardless of e.

In the following the dynamic properties of systems following the curve defined by the nullspace of (4) are analyzed.

The analysis has two components: the switching surface analysis, during which it is assumed that $s = 0$, and the boundary layer analysis, during which it is assumed that $|s| \leq \Delta_s$ for some $\Delta_s > 0$. In both cases the evolution of the position error e in time is analyzed and the smallest resting interval of e over $s \in [-\Delta_s, \Delta_s]$ is derived.
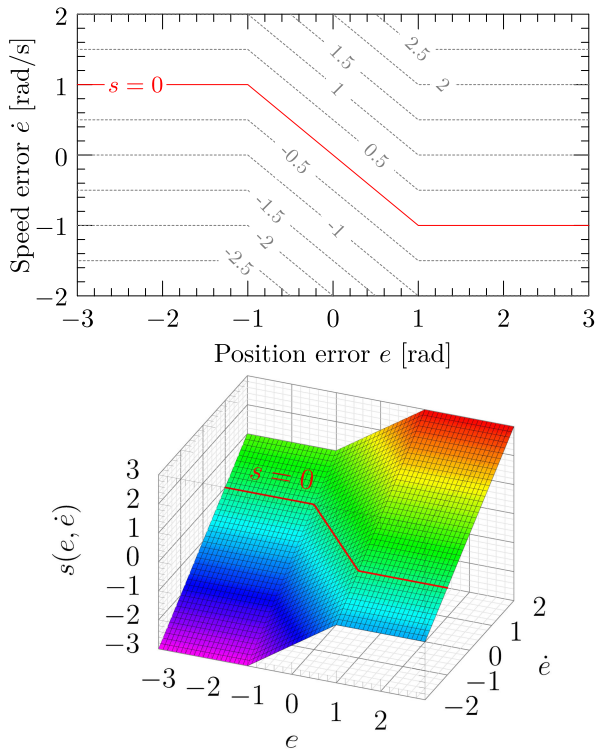
FIGURE 1. The contour plot (top) of the saturated linear switching function (SLSF) and its surface plot (bottom).

A. SATURATED LINEAR SWITCHING FUNCTION SURFACE ANALYSIS

The following lemma describes the evolution of e in time when (4) holds and $s = 0$.

Lemma 2: Let a and k be constants. If e satisfies

$$\dot{e} = -a\text{sat}(ke), \tag{5}$$

then

1) for $|e| > 1/|k|$, $d|e|/dt = -a\text{sgn}(k)$ and
2) for $|e| \leqslant 1/|k|$, e satisfies $e(t) = \exp(-akt)e(0)$.

Proof: Consider that for $|e| > 1/|k|$, it is true that $\text{sat}(ke) = \text{sgn}(ke)$, and therefore (5) is equivalent to

$$\dot{e} = -a\text{sgn}(ke) = -a\text{sgn}(k)\text{sgn}(e). \tag{6}$$

Since $e \neq 0$, then $d|e|/dt = \text{sgn}(e)\dot{e} = -a\text{sgn}(k)$, which proves 1.

Now consider that for $|e| \leqslant 1/|k|$, $\text{sat}(ke) = ke$, so that (5) reduces to $\dot{e} = -ake$, which implies $e(t) = \exp(-akt)e(0)$, which proves 2. ∎

Therefore, if $ak \leqslant 0$ and $|e| > 1/|k|$, then $d|e|/dt$ is non-negative, so that $ak > 0$ is necessary for global asymptotic stability of $e = 0$. When $ak > 0$, then $e = 0$ is globally asymptotically stable, since Lemma 2 implies that $|e|$ decreases unless $|e| = 0$ (either with constant speed or exponentially). Thus, $ak > 0$ is necessary and sufficient for asymptotic stability.

B. SATURATED LINEAR SWITCHING FUNCTION BOUNDARY LAYER ANALYSIS

When a boundary layer is used to suppress chattering, the equality $s = 0$ may or may not hold. In general, $|s|$ will be bounded, since for some s large enough in magnitude, the boundary layer control reduces to the exact (discontinuous) controller, which drives $|s|$ to zero.

The dynamics of e under the condition $|s| \leqslant \Delta_s$ for some $\Delta_s > 0$ is analyzed in this subsection. It is also assumed that both a and k are positive.

First, the influence of the boundary layer width on the speed error limit is established.

Lemma 3: Let a, k, Δ_s be positive constants and also let $s = \dot{e} + a\text{sat}(ke)$. If $|e| > 1/k$ and $|s| \leqslant \Delta_s \leqslant a$, then

$$-a - \Delta_s \leqslant \frac{d}{dt}|e| \leqslant -a + \Delta_s. \tag{7}$$

Proof: The inequalities $|e| > 1/k$, $|s| \leqslant \Delta_s \leqslant a$ and the equation $s = a\text{sat}(ke) + \dot{e}$ imply $|a\text{sgn}(ke) + \dot{e}| \leqslant \Delta_s \leqslant a$. Then the assumption that $a \geqslant \Delta_s$ results in $|a\text{sgn}(ke)| \geqslant \Delta_s$, so that $|a\text{sgn}(ke) + \dot{e}| \leqslant \Delta_s$ implies either
A.1 $\text{sgn}(e) = -\text{sgn}(\dot{e})$ if $a > \Delta_s$ or
A.2 $\dot{e} = 0$ if $a = \Delta_s$.
In case **A.1**, the expression $|a\text{sgn}(ke) + \dot{e}|$ becomes $|-\text{sgn}(\dot{e})a + \text{sgn}(\dot{e})|\dot{e}||$, where $\text{sgn}(\dot{e})$ may be factored out to get $||\dot{e}| - a|$, so that $|a\text{sgn}(ke) + \dot{e}| \leqslant \Delta_s$ becomes $||\dot{e}| - a| \leqslant \Delta_s$, which implies

$$a + \Delta_s \geqslant |\dot{e}| \geqslant a - \Delta_s, \tag{8}$$

which holds trivially for case **A.2** as well.

Since $|e| > 1/k$, then:
1) in case **A.1**, the equation $d|e|/dt = \text{sgn}(e)\dot{e} = -\text{sgn}(\dot{e})\dot{e} = -|\dot{e}|$ holds and since (8) also holds, then $-a - \Delta_s \leqslant d|e|/dt \leqslant -a + \Delta_s$, i.e. (7) holds,
2) and in case **A.2** the equation $d|e|/dt = \text{sgn}(e)\dot{e} = 0$ holds and also $a = \Delta_s$, so that (7) holds here as well.

Therefore (7) holds in both cases. ∎

Thus, for $|e| > 1/k$ the condition $a \geqslant \Delta_s$ is sufficient for $|e|$ to not increase and $a = \Delta_s + l$ with $l > 0$ is sufficient for $|e|$ to decrease with at least the speed l. It is also necessary to have $a \geqslant \Delta_s$, otherwise $|e|$ may be increasing for some $s \in [-\Delta_s, \Delta_s]$, as show in the following lemma.

Lemma 4: Let a, k, Δ_s be positive constants and define $s = a\text{sat}(ke) + \dot{e}$. If $|e| > 1/k$ and $a < \Delta_s$, then there is an $s \in [-\Delta_s, \Delta_s]$, such that $d|e|/dt > 0$.

Proof: Since $a < \Delta_s$, then $a|\text{sat}(ke)| < \Delta_s$, therefore there is an $\epsilon > 0$, such that $a|\text{sat}(ke)| + \epsilon < \Delta_s$. If $s = a\text{sat}(ke) + \text{sgn}(e)\epsilon$, then $|s| < \Delta_s$ and since $|e| > 1/k$, then $d|e|/dt = \text{sgn}(e)\dot{e} = \text{sgn}(e)[s - a\text{sat}(ke)] = \epsilon > 0$. ∎

In summary, for $a > 0$, $k > 0$ and $|e| > 1/k$ it is necessary and sufficient to have $a \geqslant \Delta_s$ in order to make sure that $d|e|/dt$ is not positive for any $s \in [-\Delta_s, \Delta_s]$ and (7) gives the bounds of $d|e|/dt$.

The next lemma establishes an exponential envelope for $e(t)$, given that $|s| \leqslant \Delta_s$ and $\Delta_s/(ak) < |e| \leqslant 1/k$, i.e. when

$|e|$ is small enough to fit into the linear region of sat(ke), but larger than $\Delta_s/(ak)$.

Lemma 5: Let a, k, Δ_s be positive constants and define $s = a\text{sat}(ke) + \dot{e}$. If $\Delta_s/(ak) < |e| \leqslant 1/k$ and $|s| \leqslant \Delta_s$, then

$$|e| \leqslant \left(|e(0)| - \frac{\Delta_s}{ak}\right)\exp(-akt) + \frac{\Delta_s}{ak}. \qquad (9)$$

Proof: Based on the assumptions $\Delta_s/(ak) < |e| \leqslant 1/k$, $s = a\text{sat}(ke) + \dot{e}$ and $|s| \leqslant \Delta_s$ it may be concluded that $|ake + \dot{e}| \leqslant \Delta_s < ak|e|$, so that $\text{sgn}(\dot{e}) = -\text{sgn}(e)$ and $ak|e| + \Delta_s \geqslant |\dot{e}| \geqslant ak|e| - \Delta_s$. Therefore, $d|e|/dt = \text{sgn}(e)\dot{e} = -|\dot{e}| \leqslant -ak|e| + \Delta_s$. Next, define $h = |e| - \Delta_s/(ak) \geqslant 0$ and observe that $d|e|/dt \leqslant -ak|e| + \Delta_s$ is equivalent to $dh/dt \leqslant -akh$, so that $h \leqslant h(0)\exp(-akt)$ [16]. Substituting $|e| - \Delta_s/(ak)$ for h gives (9). ∎

These results agree with previous results from [17] where it is stated that e converges into $[-\Delta_s/(ak), -\Delta_s/(ak)]$. See [18] for an alternative integral-based proof.

Lemma 5 shows that

$$C = \left[-\frac{\Delta_s}{ak}, \frac{\Delta_s}{ak}\right], \qquad (10)$$

is a resting interval for $e(s, t)$ over $s \in [-\Delta_s, \Delta_s]$, since $\lim_{t\to\infty}\min_{c\in C}|e(s,t) - c| = 0$ for all such s. The following lemma shows that C is also the smallest resting interval I of $e(s, t)$ over $s \in [-\Delta_s, \Delta_s]$.

Lemma 6: Let a, k, Δ_s be positive constants, define $s = a\text{sat}(ke) + \dot{e}$ and assume that s may take on any value from $[-\Delta_s, \Delta_s]$. Then,

$$I = \left[-\frac{\Delta_s}{ak}, \frac{\Delta_s}{ak}\right], \qquad (11)$$

is the smallest resting interval of $e(s, t)$.

Proof: Let I_s be a proper closed subinterval of I. Then, there is a $\epsilon \in I$, such that $\epsilon \notin I_s$. Since $\epsilon \in I$, then $|\epsilon| \leqslant \Delta_s/(ak)$, so that if $s = ak\epsilon$, then $|s| \leqslant \Delta_s$ and $ak\epsilon = a\text{sat}(ke) + \dot{e}$. Given that $e(0) \in I_s$, then $ak\epsilon = ake + \dot{e}$ and the solutions of this differential equation converge to ϵ asymptotically for all initial $e(0) \in I$. Therefore, $\lim_{t\to\infty}e(s(t), t) = \epsilon$ and based on Lemma 1 the interval I is the smallest resting interval of $e(s, t)$ over $s \in [-\Delta_s, \Delta_s]$. ∎

Lemmas 3, 5 and 6 were verified via dynamics simulation. The initial state was chosen to be $e(0) = 1$. Example trajectories for the extreme cases $s = \pm 0.1$ are given in Fig. 2. The hatched regions represent the uncertain approach regions due to speed uncertainties given by (8). The switch levels denote the moments when the dynamics switches from constant speed convergence to exponential convergence.

IV. THE SATURATED NON-SINGULAR TERMINAL SWITCHING FUNCTION

The saturated non-singular terminal switching function (SNTSF) is defined as follows:

$$s = \text{sgn}(\dot{e})|\dot{e}|^{p/q} + a\text{sat}(ke), \qquad (12)$$
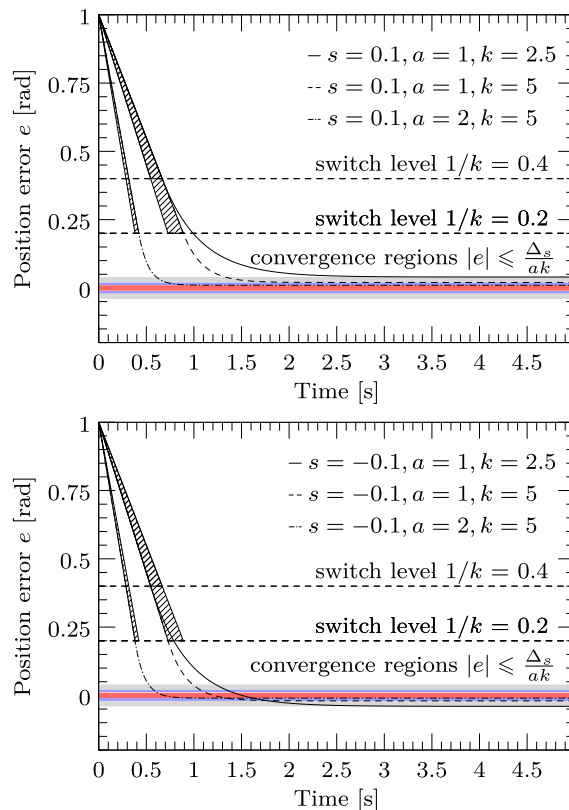
FIGURE 2. Extreme trajectories for $s = 0.1$ (top) and $s = -0.1$ (bottom) from the simulative verification of lemmas 3 and 5 under different parameter settings.

where $1 < p/q < 2$ and $a, k > 0$. This switching function is combination of the non-singular terminal switching function (NTSF) [7] and the saturation linear switching function from (4).

The contour and surface plots of the SNTSF for $a = 1$, $k = 1$, $p = 3$ and $q = 2$ are shown in Fig. 3.

The same two part analysis is carried out for the switching function (12) as was done for (4) in the previous section.

A. SATURATED NON-SINGULAR TERMINAL SWITCHING FUNCTION SURFACE ANALYSIS

Lemma 7: Assume that (12) holds. If $s = 0$ and $|e| > 1/k$, then

$$\frac{d}{dt}|e| = -a^{q/p}, \qquad (13)$$

i.e. $|e|$ converges towards 0 with the constant speed $a^{q/p}$.

Proof: For $s = 0$, the equation (12) becomes

$$\text{sgn}(\dot{e})|\dot{e}|^{p/q} = -a\text{sat}(ke). \qquad (14)$$

For $|e| > 1/k$, it is true that sat(ke) = sgn(ke), so that

$$\text{sgn}(\dot{e})|\dot{e}|^{p/q} = -a\text{sgn}(ke). \qquad (15)$$

Since $|e| > 1/k$, then sgn(ke) $\neq 0$, which implies sgn($\dot{e}$) $\neq 0$, otherwise (15) would not hold, thus

$$|\dot{e}|^{p/q} = -a\text{sgn}(ke)\text{sgn}(\dot{e}). \qquad (16)$$
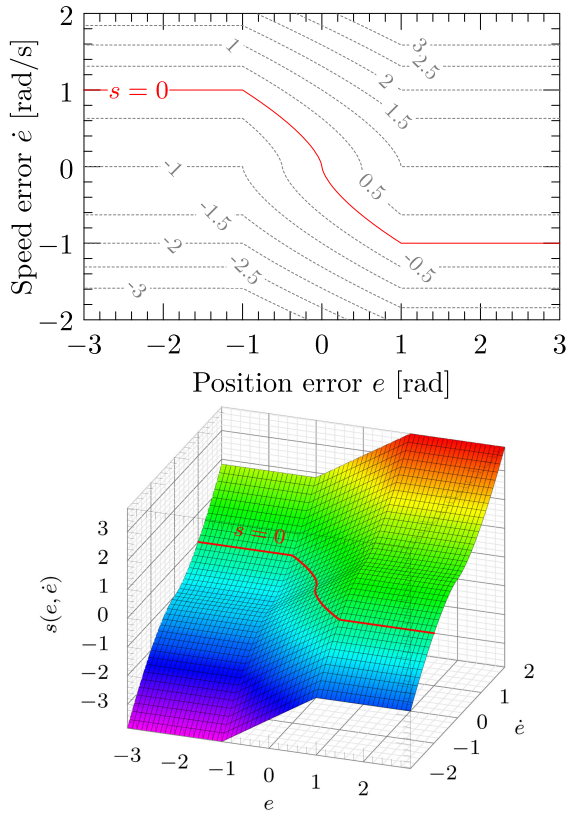
FIGURE 3. The contour plot (top) of the saturated non-singular terminal switching function (SLSF) and its surface plot (bottom).

Since a and k are positive, then $|\dot{e}| = a^{q/p}$ and $\text{sgn}(e) = -\text{sgn}(\dot{e})$. Therefore,

$$\frac{d}{dt}|e| = \text{sgn}(e)\dot{e} = -\text{sgn}(\dot{e})\dot{e} = -|\dot{e}| = -a^{q/p}. \quad (17)$$

Which completes the proof. ∎

Therefore in the case of the SNTSF, the speed limit is given by $a^{q/p}$.

For $|e| \leqslant 1/k$, equation (14) reduces to $\text{sgn}(\dot{e})|\dot{e}|^{p/q} = -ake$, therefore $e \to 0$ in finite-time [7].

B. SATURATED NON-SINGULAR TERMINAL SWITCHING FUNCTION BOUNDARY LAYER ANALYSIS

In this subsection, the boundary layer analysis of (12) is performed. It is assumed that $s = 0$ does not have to hold, but that $s \in [-\Delta_s, \Delta_s]$ for some $\Delta_s > 0$.

First, the influence of Δ_s on the speed limit $a^{q/p}$ is analyzed. The results are summarized in the following lemmas.

Lemma 8: Assume that (12) holds. If $|s| \leqslant \Delta_s$, $|e| \geqslant 1/k$ and $a > \Delta_s$, then

$$-(a + \Delta_s)^{q/p} \leqslant \frac{d}{dt}|e| \leqslant -(a - \Delta_s)^{q/p}. \quad (18)$$

Proof: Since (12) is assumed as well as $|s| \leqslant \Delta_s$, then

$$|\text{sgn}(\dot{e})|\dot{e}|^{p/q} + a\text{sat}(ke)| \leqslant \Delta_s. \quad (19)$$

Since $|e| \geqslant 1/k$, then $\text{sat}(ke) = \text{sgn}(ke)$ and therefore

$$|\text{sgn}(\dot{e})|\dot{e}|^{p/q} + a\text{sgn}(ke)| \leqslant \Delta_s. \quad (20)$$

Since $a > \Delta_s$, then

$$\text{sgn}(\dot{e}) = -\text{sgn}(ke), \quad (21)$$

since otherwise (20) would be contradicted. Equation (21) implies that

$$\frac{d}{dt}|e| = \text{sgn}(e)\dot{e} = -\text{sgn}(\dot{e})\dot{e} = -|\dot{e}|. \quad (22)$$

It also must be true that

$$||\dot{e}|^{p/q} - a| \leqslant \Delta_s, \quad (23)$$

based on (20) and (21). Inequality (23) results in

$$a - \Delta_s \leqslant |\dot{e}|^{p/q} \leqslant a + \Delta_s. \quad (24)$$

Since $a > \Delta_s$ and the function $(\cdot)^{q/p}$ for $1/2 < q/p < 1$ is monotonically increasing, then

$$(a - \Delta_s)^{q/p} \leqslant |\dot{e}| \leqslant (a + \Delta_s)^{q/p}. \quad (25)$$

Equations (22) and (25) imply (18). ∎

The following lemma describes the influence of the boundary layer width Δ_s on the convergence of e, when $\text{sat}(ke)$ is not saturated. Inside the linear region of $\text{sat}(ke)$, the SNTSF reduces to the standard NTSF [7], therefore this part of the analysis also applies to the NTSF.

Lemma 9: Assume that (12) holds. If $|s| \leqslant \Delta_s$, $|e| < 1/k$ and $ak|e| > \Delta_s$, then

$$-(ak|e| + \Delta_s)^{q/p} \leqslant \frac{d}{dt}|e| \leqslant -(ak|e| - \Delta_s)^{q/p}. \quad (26)$$

Proof: Since $|e| < 1/k$, then $\text{sat}(ke) = ke$, so that

$$|\text{sgn}(\dot{e})|\dot{e}|^{p/q} + ake| \leqslant \Delta_s. \quad (27)$$

Since $ak|e| > \Delta_s$, then

$$\text{sgn}(\dot{e}) = -\text{sgn}(e), \quad (28)$$

since otherwise (27) could not hold. Based on (28) it is true that

$$\frac{d}{dt}|e| = \text{sgn}(e)\dot{e} = -\text{sgn}(\dot{e})\dot{e} = -|\dot{e}|. \quad (29)$$

It is also true that if both (27) and (28) hold, then

$$||\dot{e}|^{p/q} - ak|e|| \leqslant \Delta_s, \quad (30)$$

which is just (27) with $|\text{sgn}(\dot{e})| = 1$ factored out. The inequality (30) implies

$$ak|e| - \Delta_s \leqslant |\dot{e}|^{p/q} \leqslant ak|e| + \Delta_s. \quad (31)$$

Since $ak|e| > \Delta_s$ and since $(\cdot)^{q/p}$ is monotonically increasing, then

$$(ak|e| - \Delta_s)^{q/p} \leqslant |\dot{e}| \leqslant (ak|e| + \Delta_s)^{q/p}. \quad (32)$$

The inequality (32) and (29) imply (26). ∎

If a and k are chosen such that the preconditions of lemmas 8 and 9 hold, then $d|e|/dt \leqslant -(ak|e| - \Delta_s)^{q/p}$ for $|e| > \Delta_s/(ak)$ and for all $s(t) \in [-\Delta_s, \Delta_s]$.

This is already sufficient for the interval

$$C = \left[-\frac{\Delta_s}{ak}, \frac{\Delta_s}{ak}\right], \qquad (33)$$

to be a resting interval of $e(s,t)$ over $s \in [-\Delta_s, \Delta_s]$.

Proof: Let $\epsilon_1, \epsilon_2 > 0$ such that $e > \Delta_s/(ak) + \epsilon_1/(ak) > \Delta_s/(ak) + \epsilon_2/(ak) > \Delta_s/(ak)$. For $e > \Delta_s/(ak) + \epsilon_2/(ak)$ it follows that $\dot{e} \leqslant -\epsilon_2^{q/p}$, so that for $e > \Delta_s/(ak) + \epsilon_1/(ak)$ it follows that $\dot{e} \leqslant -\epsilon_2^{q/p}$, because $e > \Delta_s/(ak) + \epsilon_1/(ak)$ is a subset of $e > \Delta_s/(ak) + \epsilon_1/(ak)$. Therefore, e decreases under $\Delta_s/(ak) + \epsilon_1/(ak)$, in time less than $t_1 = [e(0) - \Delta_s/(ak) - \epsilon_1/(ak)]/\epsilon_2^{q/p}$. Thus, for every $\epsilon_1 > 0$, there is a t_1, such that if $t > t_1$, then $e(t) \leqslant \Delta_s/(ak) + \epsilon_1/(ak)$.

The case when $e < -\Delta_s/(ak)$ is analogous and it shows that for every $\epsilon_1 > 0$, there is a t_1, such that if $t > t_1$, then $e(t) \geqslant -\Delta_s/(ak) - \epsilon_1/(ak)$.

Thus, for every $\epsilon_1 > 0$, there is a t_1, such that if $t > t_1$, then $|e(t)| \leqslant \Delta_s/(ak) + \epsilon_1/(ak)$, i.e. for every $\epsilon_1 > 0$, there is a t_1, such that $t > t_1$ implies $\min_{c \in C} |e(s,t) - c| < \epsilon_1/(ak)$ over all $s \in [-\Delta_s, \Delta_s]$ and thus $\lim_{t \to \infty} \min_{c \in C} |e(s,t) - c| = 0$ for all $s \in [-\Delta_s, \Delta_s]$, i.e. C is a resting set of $e(s,t)$ over $s \in [-\Delta_s, \Delta_s]$ as per Definition 1. ∎

From (7) and (18) it can be observed, that given that

$$(a + \Delta_s)^{q/p} - (a - \Delta_s)^{q/p} \leqslant 2\Delta_s \qquad (34)$$

then the bound of $d|e|/dt$ is more tight in the SNTSF case.

Equations (18) and (33) have been numerically verified by integrating (12) from the initial state $e(0) = 1$ and for the extreme cases $s = \pm\Delta_s = \pm 0.1$. The results as well as the chosen values of a, k, q and p are shown in Fig. 4. The expected resting intervals of e based on (33) are shown as shaded regions. The approach regions, that were computed based on (18), have a hatch pattern in the figure. Both (18) and (33) are verified by the simulation, since the errors converge into the corresponding regions defined by (33) and the approach speed is limited according to (18).

V. THE SMALLEST RESTING INTERVAL OF THE NON-SINGULAR TERMINAL SWITCHING FUNCTION

Lemma 6 states that (33) is the smallest resting interval of $e(s,t)$ over $s \in [-\Delta_s, \Delta_s]$ in case of the SLSF. The same interval is the smallest resting interval of $e(s,t)$ over $s \in [-\Delta_s, \Delta_s]$ for the SNTSF and the NTSF with $a > \Delta_s$, $k > 0$, $1 < p/q < 2$, based on the following lemma.

Lemma 10: Assume that

$$s = \text{sgn}(\dot{e})|\dot{e}|^{p/q} + ake, \qquad (35)$$

then

$$C = \left[-\frac{\Delta_s}{ak}, \frac{\Delta_s}{ak}\right], \qquad (36)$$

is the smallest resting interval of $e(s,t)$ over $s \in [-\Delta_s, \Delta_s]$.
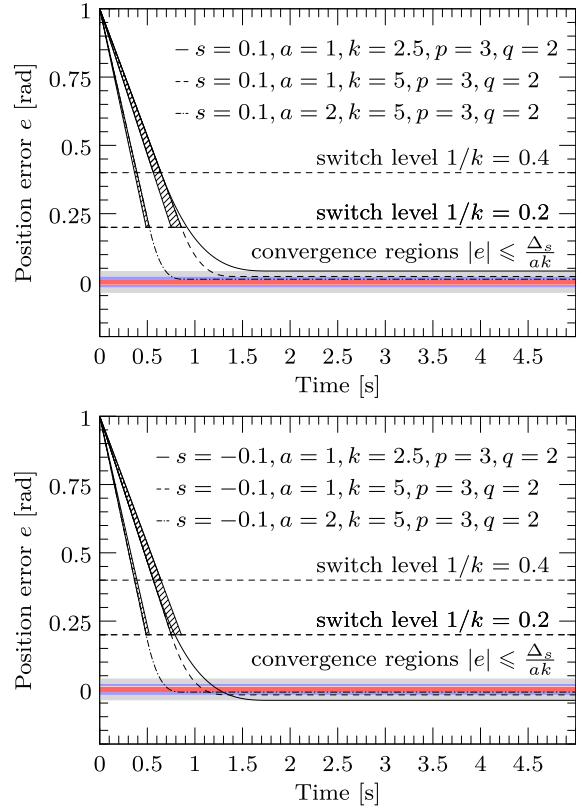
FIGURE 4. Extreme trajectories for $s = 0.1$ (top) and for $s = -0.1$ (bottom) from the simulative verification of (26) and (33).

Equation (35) holds for the NTSF and also for the SNTSF after $|e| < 1/k$, which is guaranteed to happen for $a > \Delta_s$ based on Lemma 8.

Proof: Let I_s be any closed subinterval of $I = C = [-\Delta_s/(ak), \Delta_s/(ak)]$. Then there is an ϵ, such that $\epsilon \in I$ and $\epsilon \notin I_s$. Since $\epsilon \in I$, then $|\epsilon| \leqslant \Delta_s/(ak)$. Now choose $s = ak\epsilon$, so that $|s| \leqslant \Delta_s$, i.e. $s \in [-\Delta_s, \Delta_s]$ and $\text{sgn}(\dot{e})|\dot{e}|^{p/q} + ake = ak\epsilon$. This differential equation may also be written as $\text{sgn}(\dot{h})|\dot{h}|^{p/q} = -akh$, where $h = e - \epsilon$. Since for such h, the equation $\lim_{t \to \infty} h(t) = 0$ holds, which is the same as $\lim_{t \to \infty} e = \epsilon$, so that based on Lemma 1 the interval I is the smallest resting interval of $e(s,t)$ over $s \in [-\Delta_s, \Delta_s]$. ∎

Lemma 10 contradicts some previous claims in [17] and [8] and other papers, which state that

$$I_2 = \left[-\left(\frac{\Delta_s}{ak}\right)^{p/q}, \left(\frac{\Delta_s}{ak}\right)^{p/q}\right] \qquad (37)$$

is the interval into which e converges for the NTSF given that a boundary layer of width Δ_s is used, similarly to the case of the (singular) terminal switching function (TSF).

A counterexample is provided to verify that 10 disproves (37). The following parameter settings were chosen for this experiment: $\Delta_s = 0.1$, $k = 1$, $a = 2$, $q = 2$ and $p = 3$. Convergence of e into I_2 would imply that $e \to [-0.0112, 0.0112]$ (or into $[-0.0224, 0.0224]$ in the case
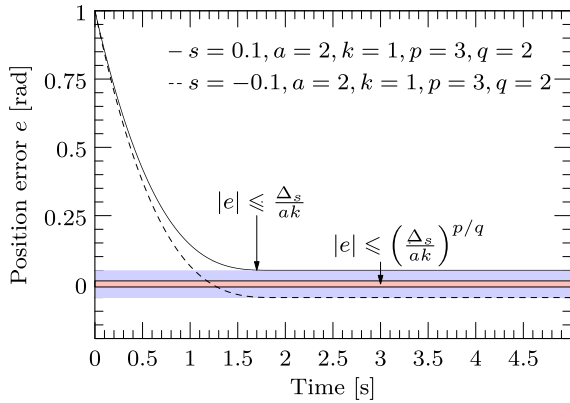
FIGURE 5. Extreme trajectories from the simulative disproof of previous claims about the steady-state error bounds in the boundary layer of non-singular terminal sliding surfaces.

of [7]), whereas convergence into I given by (33) implies $e \rightarrow [-0.05, 0.05]$. Substituting the parameters into the NTSF equation gives

$$\mathrm{sgn}(\dot{e})|\dot{e}|^{3/2} = -2e + s.\qquad(38)$$

where s may take on any value in $[-0.1, 0.1]$. This differential equation was integrated numerically for the extreme cases $s = -0.1$ and $s = 0.1$. The results are shown in Fig. 5. When integrating (38), the sign of $\dot{e}$ is $\mathrm{sgn}(-2e + s)$ and the magnitude of $\dot{e}$ is $|-2e + s|^{2/3}$. The simulation results in Fig. 5 show that the bound (37) does not hold for the non-singular terminal switching function, but that the bound (36) does, which verifies Lemma 10 and disproves the claim that e converges to (37).

The bound (37) for the NTSF was probably inferred from the properties of the TSF. Even though the NTSF and the TSF prescribe the same dynamics for $s = 0$, they have different boundary layer properties, as have been demonstrated.

VI. SATURATED NON-SINGULAR TERMINAL SLIDING MODE CONTROL

In this section, an SNTSF based controller is designed and verified for the following the second order scalar system:

$$\ddot{\theta}(\theta, \dot{\theta}, u, t) = f(\theta, \dot{\theta}, t) + b(\theta, \dot{\theta})u.\qquad(39)$$

It is assumed that θ is the position variable, $\dot{\theta} = d\theta/dt$ is the speed signal and $\ddot{\theta} = d\dot{\theta}/dt$ is the system acceleration. The reference position, speed and acceleration are denoted with r, $\dot{r}$ and $\ddot{r}$, in that order. It is also assumed that the functions f and b are not fully known, but that there are estimates $\widetilde{f}$ and $\widetilde{b}$ of f and b, respectively. Also assume that

B.1 $\Delta f_{\max} > 0$ is an upper bound of the estimation error $\Delta f = f - \widetilde{f}$,

B.2 $\Delta b_{\max} > 0$ is an upper bound of the estimation error $\Delta b = b - \widetilde{b}$ and

B.3 $|\widetilde{b}| - \Delta b_{\max} > 0$.

Using these assumptions (39) may be rewritten as

$$\ddot{\theta} = (\widetilde{f} + \Delta f) + (\widetilde{b} + \Delta b)u,\qquad(40)$$

where arguments were left out for brevity. Note, that this system is a generalization of the scalar system in [7].

The control input u for the system (40) may be chosen according to the following lemma.

Lemma 11: If assumptions **B.1**, **B.2** *and* **B.3** *hold for the system* (40) *and*

$$u = \frac{-\widetilde{f} + \ddot{r}}{\widetilde{b}} + \frac{\Delta f_{\max} + ak\frac{q}{p}|\dot{e}|^{2-\frac{p}{q}}}{|\widetilde{b}| - \Delta b_{\max}}\mathrm{sgn}(s)\mathrm{sgn}(\widetilde{b})$$
$$+ \frac{l + \Delta b_{\max}(|\widetilde{f}| + |\ddot{r}|)}{|\widetilde{b}| - \Delta b_{\max}}\mathrm{sgn}(s)\mathrm{sgn}(\widetilde{b}),\qquad(41)$$

where $l > 0$, *then* $s = 0$ *is finite-time stable, in the sense that*

C.1 s *converges to* 0 *in finite-time and*

C.2 s^2 *is non-increasing.*

Proof: Define

$$k_b = \frac{\widetilde{b} + \Delta b}{|\widetilde{b}| - \Delta b_{\max}},\qquad(42)$$

so that $\mathrm{sgn}(k_b) = \mathrm{sgn}(b)$ and $|k_b| > 1$ due to assumptions **B.2** and **B.3**, based on which $\mathrm{sgn}(b) = \mathrm{sgn}(\widetilde{b})$. Substituting (39) into $\ddot{e} = \ddot{r} - \ddot{\theta}$, then substituting (41) into the result gives

$$\ddot{e} = \ddot{r} - (\widetilde{f} + \Delta f) - (\widetilde{b} + \Delta b)\Big[\frac{-\widetilde{f} + \ddot{r}}{\widetilde{b}}$$
$$+ \frac{\Delta f_{\max} + ak\frac{q}{p}|\dot{e}|^{2-\frac{p}{q}}}{|\widetilde{b}| - \Delta b_{\max}}\mathrm{sgn}(s)\mathrm{sgn}(\widetilde{b})$$
$$+ \frac{l + \Delta b_{\max}(|\widetilde{f}| + |\ddot{r}|)}{|\widetilde{b}| - \Delta b_{\max}}\mathrm{sgn}(s)\mathrm{sgn}(\widetilde{b})\Big]$$
$$= -\Delta f - \Delta b\frac{-\widetilde{f} + \ddot{r}}{\widetilde{b}} - |k_b|\mathrm{sgn}(s)[\Delta f_{\max}$$
$$+ ak\frac{q}{p}|\dot{e}|^{2-\frac{p}{q}} + l + \Delta b_{\max}(|\widetilde{f}| + |\ddot{r}|)]$$
$$= -h\mathrm{sgn}(s) \text{ where } h \geqslant l + ak\frac{q}{p}|\dot{e}|^{2-\frac{p}{q}}.\qquad(43)$$

This is sufficient for s to converge to 0, which can be shown by considering the case when the initial error phase state $\boldsymbol{x}(0) = [e(0), \dot{e}(0)]^T$ satisfies $s > 0$ (the case $s < 0$ will also hold due to symmetry). If $s > 0$ and (43) hold, then $\ddot{e} \leqslant -l$, and therefore the phase state $\boldsymbol{x}(t) = [e(t), \dot{e}(t)]^T$ satisfies

$$\boldsymbol{x}(t) = \begin{bmatrix} e(t) \\ \dot{e}(t) \end{bmatrix} \leqslant \begin{bmatrix} e(0) + t\dot{e}(0) - \frac{1}{2}t^2 l \\ \dot{e}(0) - tl \end{bmatrix},\qquad(44)$$

which means that e is upper bounded by

$$e_{\max} = e(0) + \frac{1}{2}\frac{\dot{e}^2(0)}{l},\qquad(45)$$

Therefore, the initial phase state $\boldsymbol{x}(0)$ is in the bounded set X defined by

$$X = \{(e, \dot{e}) \text{ such that: } \mathrm{sgn}(s) > 0$$
$$\text{and } e(t) \leqslant e_{\max}$$
$$\text{and } \dot{e}(t) \leqslant \dot{e}(0) - tl\}.\qquad(46)$$

The phase state $\boldsymbol{x}(t)$ may not leave X through the boundary $e(t) = e_{\max}$, since that would contradict (44). For the same

reason, $\boldsymbol{x}(t)$ may not leave X through the boundary $\dot{e}(t) = \dot{e}(0) - tl$ either. Thus, the phase state may leave X only through the boundary $\text{sgn}(s) = 0$. The movement of the boundary $\dot{e}(t) = \dot{e}(0) - tl$ shrinks the set X and X becomes empty after a finite-time not larger than $t_f = [|\dot{e}(0)| + (ak|e_{\max}|)^{q/p}]/l$, then $\boldsymbol{x}(t)$ must have reached $\text{sgn}(s) = 0$ in finite-time. This shows **C.1**, i.e. that s converges to 0 in finite-time.

The statement **C.2** can be proven by considering two separate cases:

D.1 $\dot{e} \neq 0$ and
D.2 $\dot{e} = 0$.

In case **D.1**, i.e. when $\dot{e} \neq 0$, the derivative of $s^2/2$ w.r.t. time is

$$s\dot{s} = s\frac{p}{q}|\dot{e}|^{p/q-1}\ddot{e} + \begin{cases} 0 & \text{if } |e| \geq \frac{1}{k}, \\ sak\dot{e} & \text{if } |e| < \frac{1}{k}. \end{cases} \quad (47)$$

The definition of $\frac{d}{dt}\text{sat}(ke)$ is assumed to have been extended to the case $|e| = 1/k$, such that $\frac{d}{dt}\text{sat}(\pm 1) = 0$. If (43) is substituted into (47), then (47) becomes

$$s\dot{s} = -s\frac{p}{q}|\dot{e}|^{p/q-1}h\text{sgn}(s) + s \begin{cases} 0 & \text{if } |e| \geq \frac{1}{k} \\ ak\dot{e} & \text{if } |e| < \frac{1}{k} \end{cases}$$

$$\leq slant - l|s|\frac{p}{q}|k_b||\dot{e}|^{\frac{p}{q}-1}, \quad (48)$$

where the inequality holds because $h \geq l + akq|\dot{e}|^{2-\frac{p}{q}}/p$. Inequality (48) shows that s^2 is non-increasing for the case **D.1**.

In case **D.2**, the derivative $\dot{e}$ is zero, therefore $\dot{s} = 0$, which can be seen by differentiating (12). ∎

A. SIMULATIVE VERIFICATION

In this section, the control law (41) is verified simulatively. The testing system has the form (39) with the estimates $\widetilde{f} = 1.1\sin(t)$ rad.s^{-2}, $\widetilde{b} = 1 + 0.1\cos(t)$ rad.s^{-2}.N^{-1}.m^{-1}. Other parameters were chosen as $a = 3\text{s}^{-1}$, $k = 1$, $q = 2$, $p = 3$, $l = 0.3$. Estimation errors Δf, Δb and the chosen upper bounds $\Delta f_{\max}$, $\Delta b_{\max}$ are shown in Fig. 6. The reference signals were $r = \sin(t)$, $\dot{r} = \cos(t)$ and $\ddot{r} = -\sin(t)$ in rad, rad.s^{-1} and rad.s^{-2}, respectively. A saturation boundary layer with width $\Delta_s = 0.05$ was used to replace the sgn function in (41). This ensured that $s \leq \Delta_s$ after the reaching phase [19].

The control law (41) can also be used with the NTSF from [7], by replacing the switching function s, since the stability proof still applies. Similarly, SLSF and the LSF control laws can be obtained by choosing $p = q = 1$.

Figures 6, 7 and 8 show the comparison of SNTSF, NTSF, SLSF and LSF based controllers, all of which use the control law (41).

In the position plot in Fig. 6 (top), it can be seen, that in the case of controllers with saturated switching functions, the initial error takes longer to converge, than for the corresponding non-saturated switching function controllers.
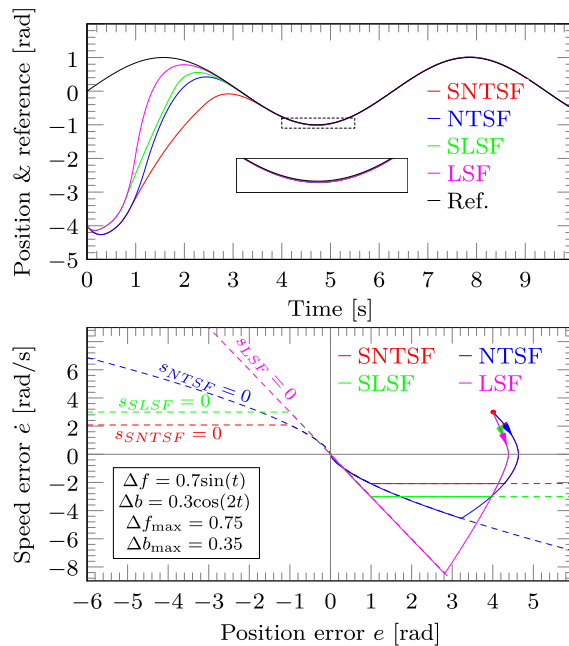
FIGURE 6. Comparison of the SNTSF, NTSF, SLSF and LSF sliding mode controllers. System position and the reference position (top) and system trajectories in the phase plane (bottom).

This is due to the limits imposed on $d|e|/dt$, as described in lemmas 3 and 8.

The $d|e|/dt$ limitation property can be seen more clearly in the phase-plane trajectory plot in Fig. 6 (bottom). In the case of the saturated switching functions, the trajectories converge to surfaces where the speed component is limited (the horizontal line segments).

In the control input plot in Fig. 7 (top) it can be seen, that the use of the saturated switching functions has resulted in smaller control amplitudes. This is as expected, since the control law (41) depends on $|\dot{e}|$ which may not increase past the speed limitation of the saturated switching functions. If the initial value of $|\dot{e}|$ is larger than the limitation, then $|\dot{e}|$ will be decreasing.

The speed error limitation property of the saturated switching functions may be observed in Fig. 7 (bottom). The speed error limitation of the saturated switching functions is not precise when a boundary layer is used as described in lemmas 3 and 8. The simulation results verify that the SNTSF has a narrower speed error uncertainty band than the SLSF for the chosen values of Δ_s, a, q and p.

In one sense, the narrower position error bound property of the terminal switching function is, in the case of the NTSF, transferred to a narrower speed error bound. The fact that the NTSF does not have the narrower boundary layer position band of the TSF is also verified by the detailed position error plot in Fig. 8.

There is no appreciable difference between the non-singular terminal and the linear switching functions when it comes to the position error bound in quasi-sliding mode, which verifies Lemma 10.
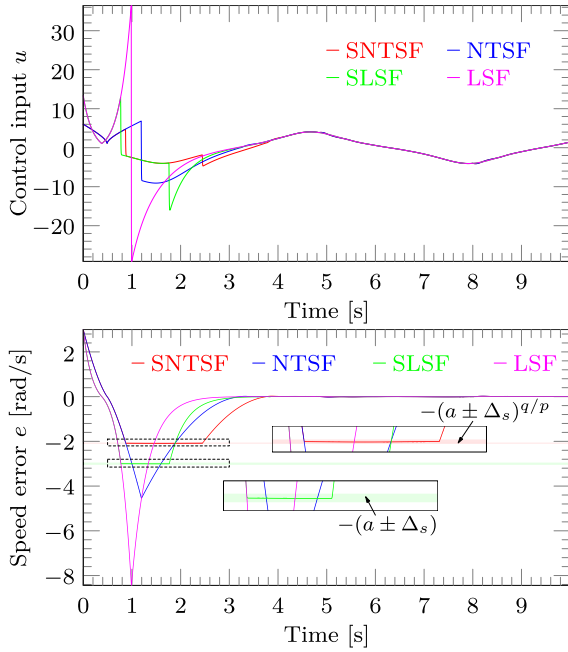
FIGURE 7. Comparison of the SNTSF, NTSF, SLSF and LSF sliding mode controllers. The controller outputs (top) and speed errors (bottom).
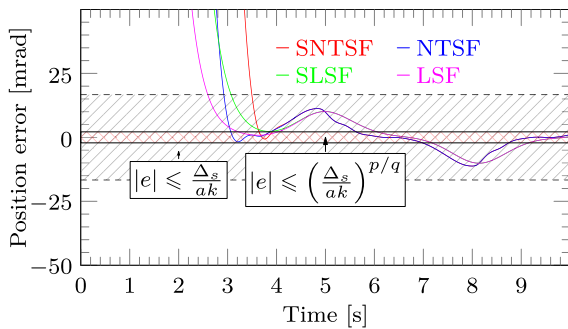
FIGURE 8. Comparison of the SNTSF, NTSF, SLSF and LSF sliding mode controllers. The position errors as functions of time.
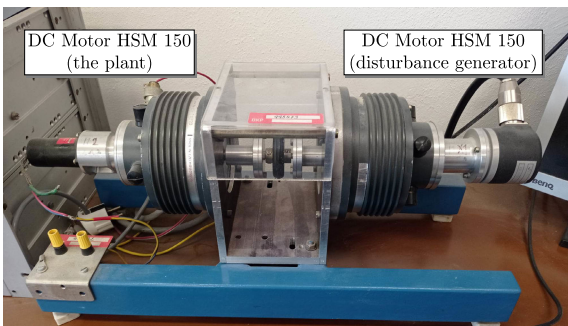
FIGURE 9. Laboratory testing equipment. The HSM150 DC motor pair.

B. LABORATORY EXPERIMENTS

Theoretical results were further verified via experiments on a laboratory system. Figure 9 shows the HSM 150 DC motor system, which was used for laboratory testing.

The following system model was assumed:

$$\ddot{\theta} = \frac{1}{j}[\text{deadz}(u, d^-, d^+) - u_d - c\dot{\theta}], \quad (49)$$

where $\ddot{\theta}$ is the angular acceleration of the motor shaft in rad.s^{-2}, $\dot{\theta}$ is the angular speed of the motor shaft in rad.s^{-1}, $c > 0$ is a friction coefficient in N.m.s.rad^{-1}, j is the total moment of inertia as seen from the motor shaft in N.m.s^2.rad^{-1}, u is the driving torque and u_d the disturbance torque in N.m. The function deadz is the deadzone function and it is defined as

$$\text{deadz}(u, d^-, d^+) = \begin{cases} 0 & \text{if } -d^- \leqslant u \leqslant d^+ \\ u + d^- & \text{if } u < -d^- \\ u - d^+ & \text{otherwise.} \end{cases} \quad (50)$$

The systems (39) and (49) are equivalent if the deadzone effect is removed and the functions f and b are defined as $f = (-u_d - c\dot{\theta})/j$ and $b = 1/j$.

The deadzone effect may be partially removed by increasing the amplitude of u by $d^+|\text{sat}(s/\Delta_s)|$ if $\text{sgn}(u) > 0$ and by $d^-|\text{sat}(s/\Delta_s)|$ if $\text{sgn}(u) < 0$.

The following system parameters were used as estimates of true values: $\tilde{j} = 1.2 \times 10^{-4}$ N.m.s^2.rad^{-1}, $\tilde{c} = 7.03 \times 10^{-5}$ N.m.s.rad^{-1}, $\tilde{d}^+ = 0.025$ N.m, $\tilde{d}^- = 0.002$ N.m, $\hat{f} = -c\dot{\theta}_f/\tilde{j}$ (where $\dot{\theta}_f$ is the filtered speed signal, which is described below) and $\tilde{b} = 1/\tilde{j}$. Switching curve and boundary layer parameters were $a = 1$ s^{-1}, $\Delta_s = 0.2$ rad.s^{-1}, $l = 8.33$, $k = 20$, $p = 3$ and $q = 2$.

The testing experiment was a small amplitude motion tracking task with an approach phase and an external disturbance effect. The reference signals were $r = 4 + 0.1\sin(t)$ rad, $\dot{r} = 0.1\cos(t)$ rad.s^{-1} and $\ddot{r} = -0.1\sin(t)$ rad.s^{-2}. A constant disturbance torque $u_d = 0.0292$ N.m was generated using the second DC motor at time $t = 10$ seconds and remained active for the rest of the experiment. This disturbance torque was accounted for using the bound Δf in (40), which should be at least $u_d/\tilde{j}$. Upper bounds of Δf and Δb were determined experimentally as $\Delta f_{\max} = 0.04/\tilde{j} = 333.33$ rad.s^{-2} and $\Delta b_{\max} = 0$ rad.s^{-1}.N^{-1}.m^{-1}.

The control scheme is shown in Fig. 10. The control law refers to (41) with the added deadzone removal algorithm.

An IRC sensor was used for position sensing and the output of the sensor was filtered using a first-order linear low-pass filter with the transfer function $1/(T_f s + 1)$ and a time constant $T_f = 0.2$ s. The output of the filter (θ_f) was numerically differentiated to obtain the filtered speed signal $\dot{\theta}_f$. The filtering was necessary to ensure the smoothness of $\dot{\theta}_f$.

The switching function value s was computed based on the filtered speed θ_f and the unfiltered position signal θ. The speed error $\dot{e}$ in the control law (41) was replaced with the filtered speed error $\dot{e}_f = \dot{r} - \theta_f$.

Figure 11 (top) shows the angular position θ during the experiments. Good position tracking was observed for each controller after the initial transient. For the saturated switching functions speed error limitation was also observed.
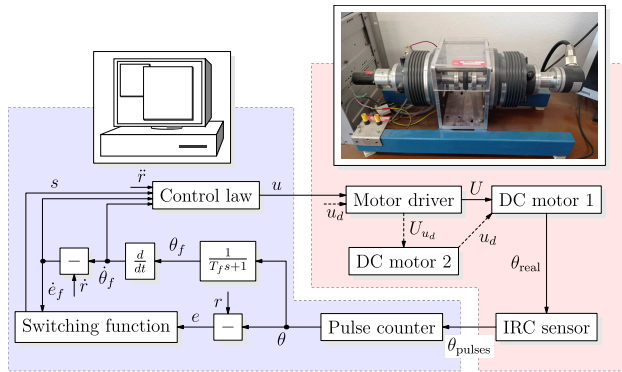
FIGURE 10. Control scheme for the laboratory experiments.
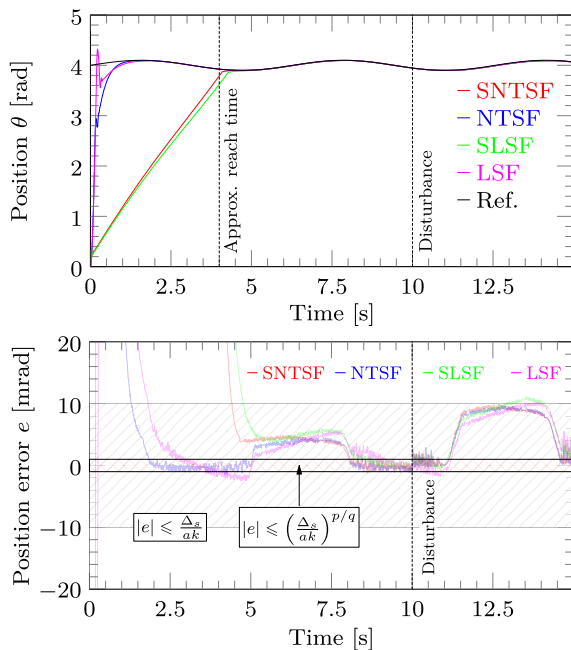
FIGURE 11. Laboratory measurement results. Position and reference signals (top) and the detailed view of the error signals (bottom).

An important property of the saturated switching functions is the fact that limiting $\dot{e}$ allows us to use larger switching function slopes with smaller control amplitudes, which can prevent overshoot in real systems with control amplitude limitations, unmodeled dynamics and filtering delays, while preserving tracking precision.

A detailed view of the position error signals is shown in Fig. 11 (bottom). It can be observed, that the position errors converged into the band (33). After the disturbance was applied, the errors remained inside or close to the band, but they left the band briefly. It is possible, that these small differences may be attributed to sensory errors, filtering and unmodeled parts of the system.

After the errors converged to their resting intervals, error trajectories remained close to each other regardless of the switching function, which verifies Lemma 10, which
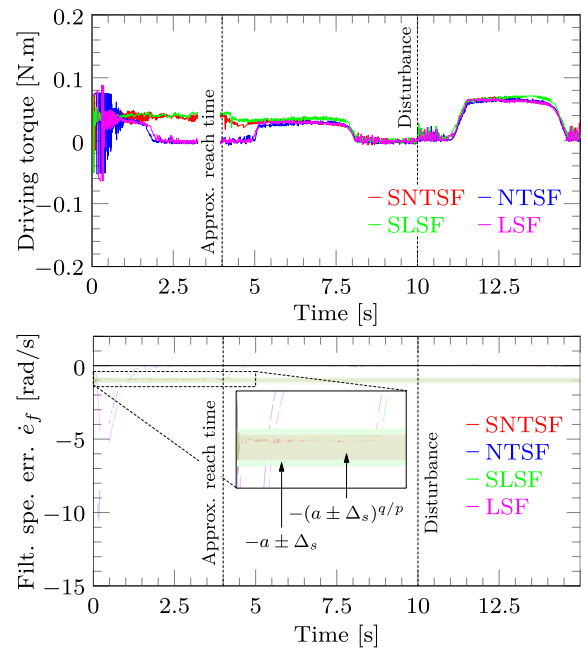
FIGURE 12. Laboratory measurement results. Controller outputs (driving torques) (top) and the speed error signals (bottom).

states that the NTSF (and SNTSF) controllers do not have a narrower smallest resting interval, than the linear switching function based controllers.

Figure 12 (top) shows the driving torques and the bottom part of Fig. 12 shows the filtered speed errors. A slight speed overshoot is present as the switching curves are reached (the red and green lines correspond to the saturated switching functions, which implement speed error limitation). This may be because of the aggressive speed signal filtering. After the overshoot, the speeds settled near in their limiting values, as described in lemmas 3 and 8.

VII. CONCLUSION
In this study, saturated variants of common switching functions were presented. The sliding-mode dynamics of these switching functions was investigated and it was demonstrated how the saturated switching functions may be used for speed error limitation.

It was shown that given the right choice of parameters the saturated non-singular terminal switching function possesses a narrower speed error (boundary layer) bound than its saturated linear counterpart. This property was exploited by designing a sliding-mode controller with a finite-time convergence guarantee and more precise speed error limitation. The controller was verified both simulatively and experimentally.

It was also proven and experimentally verified, that if a boundary layer is used, then non-singular terminal switching function based controllers do not necessarily have a higher position tracking precision than linear switching function based controllers, contrary to previous claims in the literature.

REFERENCES

[1] A. Rehman, R. Ghias, I. Ahmad, and H. I. Sherazi, "Advance optimized nonlinear control strategies for manage pressure drilling," *IEEE Access*, vol. 12, pp. 73436–73450, 2024.

[2] L. Wogi, M. Morawiec, and T. Ayana, "Sensorless control of induction motor based on super-twisting sliding mode observer with speed convergence improvement," *IEEE Access*, vol. 12, pp. 74239–74250, 2024.

[3] W. Chen, D. Tao, and B. Tang, "A new reaching law based nonsingular terminal sliding mode control scheme for the servo system with periodic uncertainties," *IEEE Access*, vol. 12, pp. 64461–64472, 2024.

[4] Y. Shtessel, C. Edwards, L. Fridman, and A. Levant, *Sliding Mode Control and Observation* (Control Engineering). New York, NY, USA: Springer, 2013, doi: 10.1007/978-0-8176-4893-0.

[5] S. Tokat, M. S. Fadali, and O. Eray, *A Classification and Overview of Sliding Mode Controller Sliding Surface Design Methods*. Cham, Switzerland: Springer, 2015, pp. 417–439, doi: 10.1007/978-3-319-18290-2_20.

[6] V. Utkin, "Variable structure systems with sliding modes," *IEEE Trans. Autom. Control*, vol. AC-22, no. 2, pp. 212–222, Apr. 1977.

[7] Y. Feng, X. Yu, and Z. Man, "Non-singular terminal sliding mode control of rigid manipulators," *Automatica*, vol. 38, no. 12, pp. 2159–2167, Dec. 2002. [Online]. Available: https://www.sciencedirect.com/science/article/pii/S0005109802001474

[8] X. Yu, Y. Feng, and Z. Man, "Terminal sliding mode control—An overview," *IEEE Open J. Ind. Electron. Soc.*, vol. 2, pp. 36–52, 2021.

[9] Z. Yang, D. Zhang, X. Sun, W. Sun, and L. Chen, "Nonsingular fast terminal sliding mode control for a bearingless induction motor," *IEEE Access*, vol. 5, pp. 16656–16664, 2017.

[10] Y. Kim, H. Ahn, M. Hu, and K. You, "Improved non-singular fast terminal sliding mode control for SPMSM speed regulation," *IEEE Access*, vol. 11, pp. 65924–65933, 2023.

[11] C. Xiu and P. Guo, "Global terminal sliding mode control with the quick reaching law and its application," *IEEE Access*, vol. 6, pp. 49793–49800, 2018.

[12] J. Kardoš, "Robust point-to-point control with velocity limitation," in *Proc. 21st Int. Conf. Process Control (PC)*, Strbske Pleso, Slovakia, Jun. 2017, pp. 81–85.

[13] C. A. Martínez-Fuentes, U. Pérez-Ventura, and L. Fridman, "Chattering analysis for Lipschitz continuous sliding-mode controllers," *Int. J. Robust Nonlinear Control*, vol. 31, no. 9, pp. 3779–3794, Jun. 2021.

[14] M.-S. Chen, Y.-R. Hwang, and M. Tomizuka, "A state-dependent boundary layer design for sliding mode control," *IEEE Trans. Autom. Control*, vol. 47, no. 10, pp. 1677–1681, Oct. 2002.

[15] J. C. Bowman and O. Shardt, "Asymptote: Lifting TEX to three dimensions," *TUGboat, Commun. TEX Users Group*, vol. 30, no. 1, pp. 58–63, 2009.

[16] J. Slotine and W. Li, *Applied Nonlinear Control*. Upper Saddle River, NJ, USA: Prentice-Hall, 1991.

[17] Y. Feng, X. Yu, and F. Han, "On nonsingular terminal sliding-mode control of nonlinear systems," *Automatica*, vol. 49, no. 6, pp. 1715–1722, Jun. 2013.

[18] D. Vasko, J. Kardoš, and E. Miklovièová, "Variable structure control of second order systems with nonlinear uncertain discontinuous input functions using approximate inverses," *IEEE Access*, vol. 10, pp. 134157–134163, 2022.

[19] F. Wang, J. Wang, K. Wang, C. Hua, and Q. Zong, "Finite-time control for uncertain systems and application to flight control," *Nonlinear Anal., Model. Control*, vol. 25, no. 2, pp. 163–182, Mar. 2020.

DENIS VASKO was born in Slovakia, in 1997. He received the B.Sc. and M.Sc. degrees in cybernetics from the Faculty of Electrical Engineering and Information Technology, Slovak University of Technology in Bratislava, Bratislava, in 2019 and 2021, respectively, where he is currently pursuing the Ph.D. degree. His research interests include variable structure control, Lyapunov design approach, and soft computing.

JÁN KARDOŠ received the M.Sc. and Ph.D. degrees in cybernetics and automation from Slovak University of Technology in Bratislava (STU), Slovakia, in 1976 and 2004, respectively. Since 2012, he has been an Associate Professor with the Institute of Robotics and Cybernetics, Faculty of Electrical Engineering and Information Technology, STU. His research interests include the theory of control in robotics and mechatronics, particularly the robust variable structure control of motion systems.

EVA MIKLOVIČOVÁ received the M.Sc. and Ph.D. degrees in automation from Slovak University of Technology in Bratislava (STU), in 1990 and 1997, respectively. She is currently an Associate Professor with the Institute of Robotics and Cybernetics, Faculty of Electrical Engineering and Information Technology, STU. Her research interests include predictive control, adaptive control, system modeling, and identification.

ĽUBOŠ CHOVANEC was born in Trenčín, Slovakia, in 1985. He received the M.Sc. degree in robotics and the Ph.D. degree in automation and control from Slovak University of Technology in Bratislava, in 2010 and 2017, respectively. His research interests include motion control of low-damped mechatronics systems, algorithms for visual systems, servo control, and real-time systems.

• • •